

Electronic Supplementary Information

Layered cobalt oxide epitaxial films exhibiting thermoelectric $ZT = 0.11$ at room temperature

Yugo Takashima,^a Yu-qiao Zhang,^{*b} Jiake Wei,^{c,d} Bin Feng,^c Yuichi Ikuhara,^{c,d} Hai Jun Cho,^{a,b} and Hiromichi Ohta^{*a,b}

Author affiliations

* Corresponding authors

^aGraduate School of Information Science and Technology, Hokkaido University,
N14W9, Kita, Sapporo 060–0814, Japan

^bResearch Institute for Electronic Science, Hokkaido University, N20W10, Kita,
Sapporo 001–0020, Japan

E-mail: yuqiaozhang0730@gmail.com

E-mail: hiromichi.ohta@es.hokudai.ac.jp

^cInstitute of Engineering Innovation, The University of Tokyo, 2–11–16 Yayoi, Bunkyo,
Tokyo 113–8656, Japan

^dElements Strategy Initiative for Structural Materials, Kyoto University, Yoshida-
honmachi, Sakyo-ku, Kyoto 606–8501, Japan

Table S1. Thermoelectric properties of the layered cobaltite epitaxial films in the in-plane direction at room temperature. In addition to the observed properties, we calculated the lattice thermal conductivity ($\kappa_{\text{lattice}} = \kappa_{\text{obsd}} - \kappa_{\text{electron}}$). The electron thermal conductivity (κ_{electron}) was estimated by assuming the Wiedemann-Franz law ($\kappa_{\text{electron}} = L \cdot \sigma \cdot T$, where the L is $2.44 \times 10^{-8} \text{ W } \Omega \text{ K}^{-2}$).

	$\text{Ca}_{1/3}\text{CoO}_2$ ¹⁹	$\text{Na}_{0.75}\text{CoO}_2$	$\text{Sr}_{1/3}\text{CoO}_2$ ²¹	$\text{Ba}_{0.27}\text{CoO}_2$
σ_{in} (S cm ⁻¹)	1330	1330	890	2310
S_{in} ($\mu\text{V K}^{-1}$)	+90	+96	+115	+72
PF_{in} (mW m ⁻¹ K ⁻²)	1.08	1.23	1.18	1.20
$\kappa_{\text{in obsd}}$ (W m ⁻¹ K ⁻¹)	6.79	5.46	4.51	3.29
$\kappa_{\text{in electron}}$ (W m ⁻¹ K ⁻¹)	0.98	0.97	0.65	1.69
$\kappa_{\text{in lattice}}$ (W m ⁻¹ K ⁻¹)	5.81	4.49	3.86	1.60
ZT_{in}	0.048	0.067	0.078	0.11

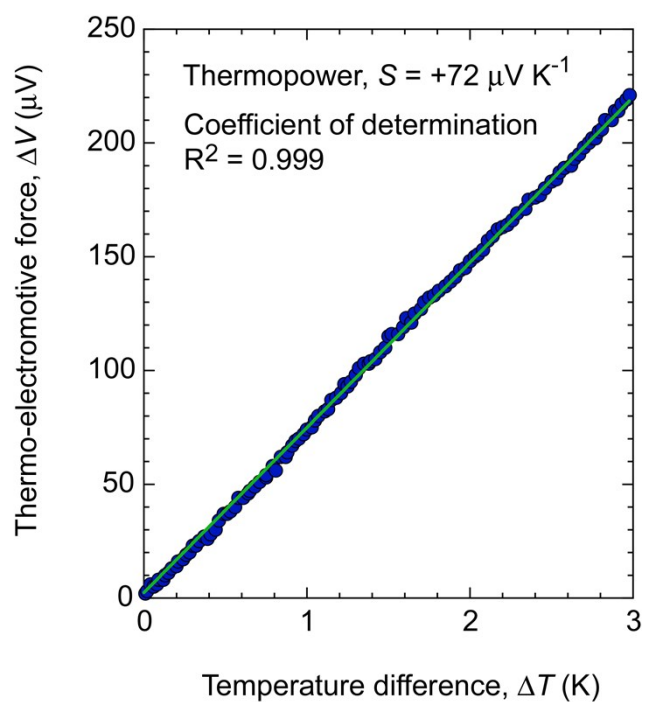


Figure S1. Typical thermo-electromotive force (ΔV) vs. temperature difference (ΔT) plot of the resultant $\text{Ba}_{0.27}\text{CoO}_2$ epitaxial film at room temperature. The thermopower (S) was calculated to be $+72 \mu\text{V K}^{-1}$ as the linear slope of the $\Delta T - \Delta V$ plot. The coefficient of determination (R^2) was 0.999.

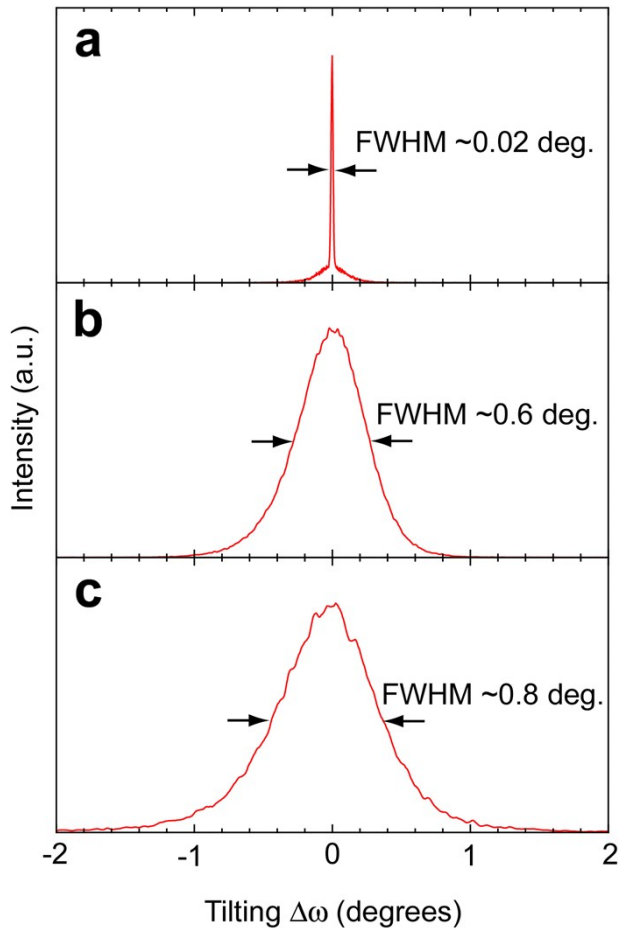


Figure S2. Average crystal tilting of the resultant films in the out-of-plane direction. Out-of-plane X-ray rocking curves of (a) 111 CoO after step 1, (b) 0002 $\text{Na}_{0.75}\text{CoO}_2$ after step 2, and (c) 0002 $\text{Ba}_{1/3}\text{CoO}_2$ after step 3. The full-width at half maximum (FWHM) values are (a) $\sim 0.02^\circ$, (b) $\sim 0.6^\circ$ and (c) $\sim 0.8^\circ$, respectively. Since the topographic AFM images of these films [Figs. 3(d)–(f)] show grain growth tendency, the increasing tendency of the FWHM values reflects the warp of the films, not mosaicity.

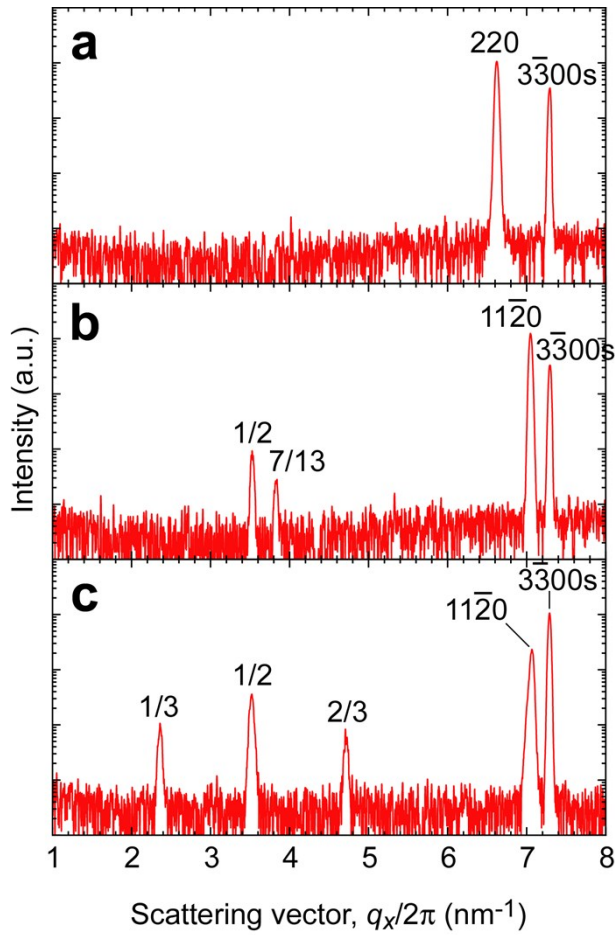


Figure S3. Change in the in-plane XRD pattern of the resultant films on (0001) $\alpha\text{-Al}_2\text{O}_3$ substrate. (a) After step 1 (CoO), (b) after step 2 ($\text{Na}_{0.75}\text{CoO}_2$), and (c) after step 3 ($\text{Ba}_{1/3}\text{CoO}_2$). The epitaxial relationship of (a) is $(111)[110]$ CoO \parallel $(0001)[1-100]$ $\alpha\text{-Al}_2\text{O}_3$, (b) is $(0001)[1-120]$ $\text{Na}_{0.75}\text{CoO}_2$ \parallel $(0001)[1-100]$ $\alpha\text{-Al}_2\text{O}_3$, and (c) is $(0001)[1-120]$ $\text{Ba}_{1/3}\text{CoO}_2$ \parallel $(0001)[1-100]$ $\alpha\text{-Al}_2\text{O}_3$, respectively. Several diffraction peaks due to sublattices of Na ($1/2$ and $7/13$) and Ba ($1/3$, $1/2$, and $2/3$) are clearly seen in (b) and (c).

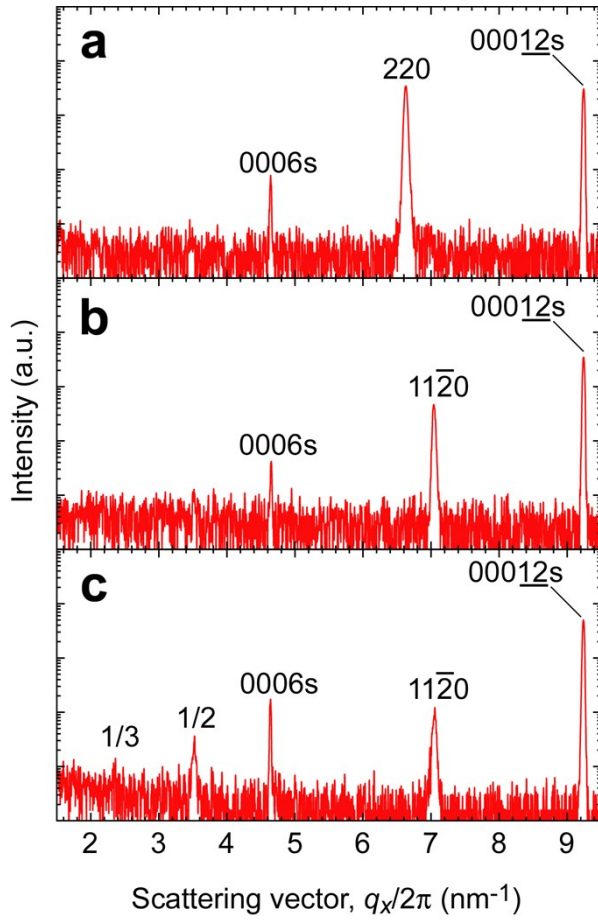


Figure S4. Change in the in-plane XRD pattern of the resultant films on (1-100) α - Al_2O_3 substrate. (a) After step 1 (CoO), (b) after step 2 ($\text{Na}_{0.75}\text{CoO}_2$), and (c) after step 3 ($\text{Ba}_{1/3}\text{CoO}_2$). The epitaxial relationship of (a) is $[110]$ CoO \parallel $[0001]$ α - Al_2O_3 , (b) is $[1-120]$ $\text{Na}_{0.75}\text{CoO}_2$ \parallel $[0001]$ α - Al_2O_3 , and (c) is $[1-120]$ $\text{Ba}_{1/3}\text{CoO}_2$ \parallel $[0001]$ α - Al_2O_3 , respectively. Several diffraction peaks due to sublattices of Ba (1/3 and 1/2) are clearly seen in (c).

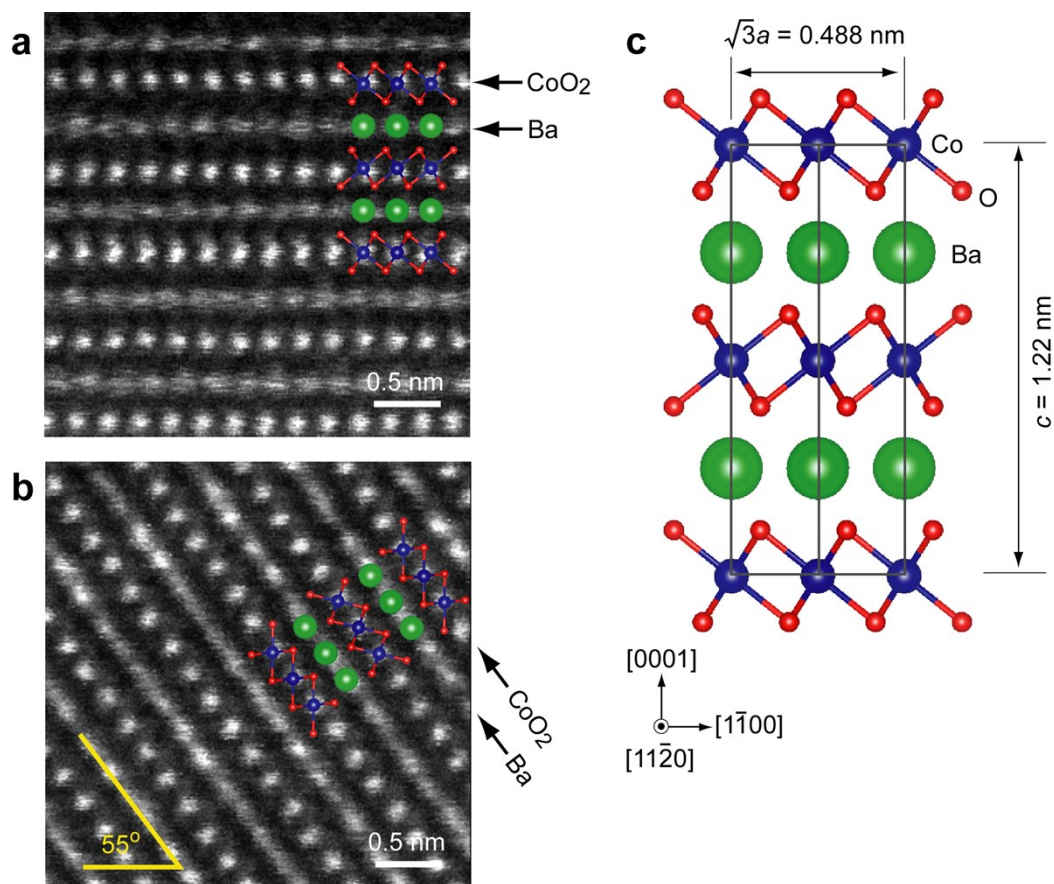


Figure S5. The atomic arrangement of the Ba_{0.27}CoO₂ films. The magnified HAADF-STEM image of the film grown on (a) (0001) α -Al₂O₃ substrate and (b) (1-100) α -Al₂O₃ substrate. The schematic crystal structure of Ba_{1/3}CoO₂ (c) is superimposed in the STEM images. The Ba and CoO₂ layers are stacked parallel to the (0001) substrate surface whereas Ba and CoO₂ layers are inclined 55° to the (1-100) substrate surface.

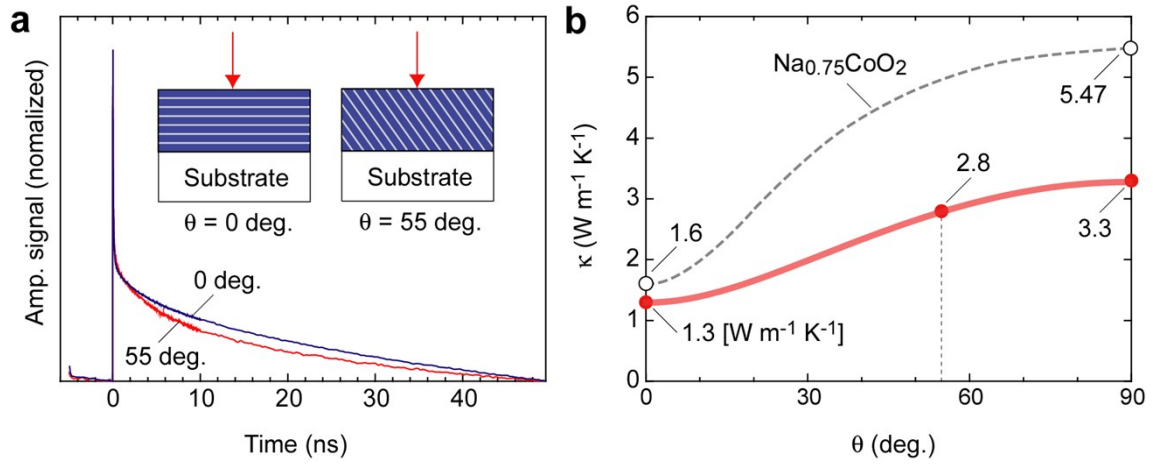


Figure S6. Thermal conductivity of the $\text{Ba}_{0.27}\text{CoO}_2$ epitaxial films at room temperature. (a) Decay curves of TDTR signal. The 55° inclined film shows faster decay. (b) Thermal conductivity of the $\text{Ba}_{0.27}\text{CoO}_2$ epitaxial films. The observed thermal conductivity of the c -axis oriented $\text{Ba}_{0.27}\text{CoO}_2$ epitaxial film ($\theta = 0^\circ$) was $1.3 \text{ W m}^{-1} \text{ K}^{-1}$ and that of the 55° inclined film was $2.8 \text{ W m}^{-1} \text{ K}^{-1}$. The thermal conductivity along the CoO_2 layer ($\theta = 90^\circ$) was obtained theoretically using these values.